Hindawi
Shock and Vibration
Volume 2020, Article ID 8813024, 14 pages
https://doi.org/10.1155/2020/8813024

Research Article

Experimental Study on Inverse Model-Based Force Tracking Control of MR Damper

Shuli Wei,[1] Jian Wang ,[2,3] and Jinping Ou[1,2,3]

[1]*School of Civil and Environment Engineering, Harbin Institute of Technology, Shenzhen, China*
[2]*Key Lab of Structures Dynamic Behavior and Control of the Ministry of Education, Harbin Institute of Technology, Harbin, China*
[3]*Key Lab of Smart Prevention and Mitigation of Civil Engineering Disasters of the Ministry of Industry and Information Technology, Harbin Institute of Technology, Harbin, China*

Correspondence should be addressed to Jian Wang; wangjiantx@hit.edu.cn

Received 24 July 2020; Revised 4 September 2020; Accepted 10 September 2020; Published 21 September 2020

Academic Editor: Mohammad Rafiee

An explicit inverse model of a magnetorheological (MR) damper is established to track the desired force in real time through experimental analysis and mathematical modeling. An algebraic hyperbolic tangent model is used to present the nonlinear behavior of MR dampers to avoid dynamic evolution due to effortless invertibility. A characteristic method is utilized to obtain the initial parameters of this algebraic hyperbolic tangent model; subsequently, the main parameters of the algebraic model are selected as quadratic functions of the applied current such that the closed-form expressions of the inverse model can be obtained. Then, the response time including communication and electromagnetic interactions in the experiment is investigated and modeled. By combining the force-current and electromagnetic models, an inverse model-based force tracking scheme is proposed. A series of validated tests are performed to study the force tracking performance. The proposed model exhibits high fidelity for tracking variable desired forces in experiments. Further analysis on force tracking errors demonstrates the mitigation of errors in various current fluctuating methods.

1. Introduction

A magnetorheological (MR) damper integrates a special fluid that contains polarizable particles into an ordinary fluid damper. The yield stress of the fluid can be changed significantly by adjusting the magnitude of an applied magnetic field produced by the coil. As the yield strength of the fluid depends on the level of applied current in the coil, this relationship renders the MR damper a controllable fluid damper and only a small current is required. Because an MR damper is controllable and versatile, it has garnered significant attention.

The main operation of the MR damper in semiactive control is the determination of the command current according to an appropriate control algorithm [1–3]. Most applications and experimental studies in this context have been completed through various ON-OFF control algorithms [4]. The clipped-optimal control, as the widest semiactive control method for MR dampers, is a typical ON-OFF control algorithm. This method applies the step current into MR dampers to approximately generate the desired force, not to derive the real-time current. The force tracking control is rarely used to produce a command force precisely. The main barrier to achieve the force tracking control is the complex dynamic behavior of MR dampers, especially in the vicinity of small velocities. The compressibility, nonlinear shear behavior, and inertia of MR fluids may complicate the fluid dynamics. Meanwhile, other experimental factors, such as time delay and dynamic response of electromagnetic or MR fluids, may increase modeling errors. Therefore, the force tracking control of an MR damper must be developed to realize a versatile damper.

To realize the force tracking control of an MR damper, an inverse model control based on the dynamic model of an

MR damper is the most straightforward and convenient method, intuitively. The model of an MR damper can be classified as parametric and nonparametric models; hence, inverse model control is developed in these two models. According to whether dynamic states exist, the parametric model can be categorized into static hysteretic models such as the Bingham and algebraic hyperbolic tangent models [5, 6] and dynamic hysteretic models such as the Bouc–Wen hysteresis [7–9] and dynamic magnetic circuit models [10]. However, owing to its nonlinear characteristics, the inverse dynamics model cannot be derived analytically. The use of additional hysteretic variables in the dynamic model renders such models irreversible for real-time control purposes. Inverse dynamics models have been developed for both the Bingham and Bouc–Wen models to track the desirable control forces. Based on the approximate exponential relationship between the yield force of an MR damper and applied current, the required current is obtained, and hence the desired damper force is generated. It is noteworthy that significant errors exist in the preyield region owing to such an approximation, while good accuracy can be achieved for larger yield stresses in the postyield region [11]. The damper force has been formulated as the product of current gain and passive hysteresis force. The passive hysteresis force is assumed to be current independent to derive the inverse model of an MR damper. Based on this inverse model, an asymmetric damping force generation algorithm is proposed to realize desired variable and asymmetric damping characteristics [12]. These published studies regarding inverse dynamic models have never been validated experimentally.

Unlike the complex mathematical formulas and difficult inverse derivations of parametric models, nonparametric models have been developed well in recent years, primarily based on artificial neural network [13–15] and fuzzy logical [16, 17] and neural-fuzzy approaches [18]. Both forward and inverse models based on recurrent neural networks with history information inputs have been constructed to emulate MR damper dynamics by Chang et al. [19]. Numerical results show that RNN models can achieve good performances and the desirable optimal control force. The inverse model of an MR damper [20] has been developed using optimal neural network and system identification techniques, which was trained and validated with simulated data considering previous input voltages; the validated results demonstrate a good prediction for the voltage of the desired force. Ni et al. [21] utilized the NARX network to formulate an inverse dynamic model for a self-sensing MR damper, where the NARX model considered past values of the applied current as input to predict the present applied current. The validation results indicated a good agreement between the measured and predicted damper forces. However, the aforementioned NN models with history information inputs regarding current or voltage required an additional sensor to gather the current or voltage in real time, which increased the architecture size and the instrumentation cost of a control system and computing time. Unlike those methods, Bani-Hani and Sheban [22] proposed an inverse model without history voltage input to replicate the inverse dynamics of an MR damper to track the desired force generated from the LQG control algorithm, in which the predicted voltages are approximately the target voltages. However, the training and validation data were generated from a given formula, and the performance of this model was not validated for experimental data. Weber et al. [23] constructed an inverse model using an artificial neural network to perform force tracking. The predicted current exhibited unreasonable spikes during velocity zero crossings. To compensate the errors of inverse artificial neural network models, PI control [24] has been introduced to improve the track accuracy and robustness performance, where the actual and integral errors were considered to yield an efficient and robust scheme. The damper force provides real-time feedback to calculate the actual and integral errors for current correction. Metered et al. [25] compared the accuracy of an inverse model with and without the voltage input history using an RNN. The results are unsatisfactory when the inverse RNN model does not include the voltage input history. Therefore, although nonparametric models are the most powerful to capture the complex nonlinearity, existing studies have not shown its advantage in addressing the inverse dynamics of MR dampers if an additional current sensor is used.

In addition to the inverse model control, other force tracking schemes are the force-feedback type developed using the model control theory. A force-feedback approach of switching between a controller block and a back-driven block has been proposed for different situations and shown to be effective [26]. A PI controller with a large proportional gain was utilized to track the realizable desired force in the controller block. Based on the real-time feedback force, a piecewise linear interpolation method has been adopted to obtain the applied current [27]. This interpolation method can be used directly according to experimental data without the fitting parametric model. A static hysteresis model [28] in algebraic expressions has been used to describe the dynamic behavior of MR dampers for avoiding intractable internal nonlinear dynamics. Based on this model, a second-order sliding mode controller has been developed to determine the applied current via the time rate of the current change. Based on the force tracking capacity, a semiactive vibration absorber with a real-time adaptive nonlinear controlled MR damper (MR-SVA) for the mitigation of harmonic structural vibrations has been presented, and the MR-SVA can be tuned correctly to the targeted structural resonance frequency, as validated by simulations and experiments [29].

Herein, an explicit inverse model of an MR damper is proposed to track the desired force in real time. First, a reliable methodology to obtain the initial value of the parameters of the hyperbolic tangent model is derived to retain the characteristics of each parameter. Subsequently, the estimated parameters are refined as the lower-order function of the current to transform the constant-current model for time-varying currents. The response time including communication and electromagnetic interactions in the experiment is investigated and modeled. Finally, a model-based real-time force tracking scheme is introduced and validated. A detailed analysis is provided to distinguish the source of force tracking errors.

2. Force-Current Model Based on Hyperbolic Tangent Function

In this study, the algebraic hyperbolic tangent model was selected for modeling an MR damper. This model could evolve easily into the function of applied current (refer to the force-current model) and can provide a closed-form solution of force in the MR damper. Its drawback is the lack of a few frequency-dependent behaviors. However, owing to its invertibility, this model can be developed to conduct force tracking control. The damping force f derived from the model can be expressed as

$$f = f_y \tanh\left(a_1\dot{x} + a_2 x\right) + c\dot{x} + kx + f_0, \tag{1}$$

where the first term (hysteretic component) describes the hysteretic behavior in the low-velocity region and presents the level of yield force; f_y is the yield force level of the hysteretic component; and α_1 and α_2 are the arguments of the hyperbolic tangent function to capture the hysteretic behavior in the low-velocity region. The second term (dashpot component) describes the velocity-dependent behavior in the high-velocity region, and c is the viscous coefficient of the dashpot. The third term is the stiffness term (spring component) to describe the compressed gas in the accumulator, where k is the stiffness coefficient of the spring; f_0 is the offset of damper force; and $\dot{x}$ and x are the piston velocity and displacement, respectively.

2.1. Characteristic Parameters for Algebraic Hyperbolic Tangent Model. This methodology is based on the effect of each parameter on the hysteresis loop. It can provide more suitable initial values of these parameters for improving the estimated accuracy and time consumption; additionally, it can maintain the characteristics of each parameter. Figure 1 shows a typical force-velocity curve with the characteristic points of an MR damper. The points $P_0(\dot{x}_0, 0)$, $P_c(0, f_c)$ are defined at the position on the upper line (soild line) where the force is zero and velocity is zero, respectively. $P_i(\dot{x}_i, f_i)$ is located at the intersection of the upper and lower line (dotted line). The point where force reaches maximum is defined as $P_m(\dot{x}_m, f_m)$. All those points are marked by red dot in Figure 1.

The yield force level of the hysteretic component is dependent on the yield of the MR fluid, which may be extracted from point P_c. The viscous component dominates the slope of the force-velocity relationship in the high-velocity region. Therefore, the viscous coefficient can be extracted from the typical hysteresis loop, where its centerline reaches the maximum velocity. Using points P_m and P_i, the centerline slope of the force-velocity relationship in the high-velocity region can be well approximated by the following equation:

$$c = \frac{f_m - f_i}{\dot{x}_m - \dot{x}_i}. \tag{2}$$

The arguments of the hyperbolic tangent function can capture the hysteretic behavior in the low-velocity region. To some extent, argument α_1 has more effect on the slope of the hysteresis loop in the low-velocity region. The slope of the hysteretic loop can be calculated using points P_c and P_0. By considering the partial derivative of the damper force with respect to velocity, the slope can be approximated as

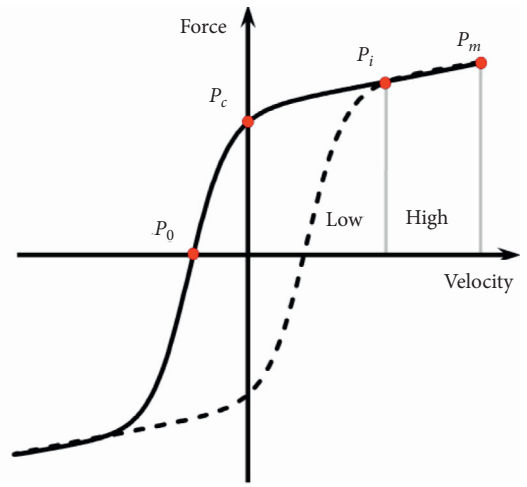

Figure 1: Characteristic points in typical force-velocity curve.

$$\frac{\partial f}{\partial \dot{x}} \approx c + f_y a_1. \tag{3}$$

Based on equation (3) and the actual slope of the hysteretic loop in the low-velocity region, argument α_1 can be obtained.

Assuming that the damping force is equal to zero, equation (1) can be written as

$$a_1\dot{x} + a_2 x = \frac{1}{2}\ln\frac{f_y - f_l}{f_y + f_l}, \tag{4}$$

where internal variable $f_l = c\dot{x} + kx + f_0$; subsequently, Taylor expansion is applied on the right-hand term of equation (4) and the higher-order terms are ignored. Therefore, equation (4) can be approximated as

$$a_1\dot{x} + a_2 x + \frac{f_l}{f_y} = 0 \tag{5}$$

Assume that f_l is significantly less than f_y in the low-velocity region; therefore,

$$a_2 \approx -\frac{a_1\dot{x}}{x}. \tag{6}$$

The stiffness component dominates the slope of the force-displacement relationship in the high-velocity region, which can induce different behaviors of both motion directions in the high-velocity region. The stiffness coefficient [9] can be calculated by

$$k = \frac{\dot{x}_m\left(f_{iu} - f_{il}\right)}{2x_m\sqrt{\dot{x}_m^2 - \dot{x}_i^2}}, \tag{7}$$

where x_m represents the maximum displacement; $\dot{x}_i$ represents the velocities at point i in the vicinity of the

maximum velocity; and f_{iu} and f_{il} represent the force at the upper and lower curves (dashed line) of the hysteresis loop when the velocity is $\dot{x}_i$, respectively. The offset of damper force can be well approximated by the mean value of the maximum damper force at positive and negative velocities.

2.2. Validation of Model for Constant Current Input. The methodology explained above is applied to obtain the parameters of the algebraic hyperbolic tangent model for sinusoidal excitations. The fitness objective function is evaluated as the root-mean-square error (RMSE) between the measured and simulated damper forces:

$$\mathrm{RMSE} = \sqrt{\frac{\sum_{j=1}^{N} \left(f_{\mathrm{act}}^{j} - f_{\mathrm{sim}}^{j}\right)^2}{\sum_{j=1}^{N} \left(f_{\mathrm{act}}^{j}\right)^2}}, \tag{8}$$

where N is the number of data points and f_{act}^{j} and f_{sim}^{j} are the actual force in the experiments and the simulated force of the algebraic hyperbolic tangent model, respectively.

An error comparison with the estimated (Est.) results from the characteristic method above and the fitting (Fit.) results, which applies the estimated parameters as initial values, is shown in Table 1. The expression "Sin1 Hz5 mm" represents that the frequency of sinusoidal excitation is 1 Hz and the amplitude is 5 mm, and the other expressions in Table 1 are similar to it. The RMSE of estimated results is ~10%, and the RMSE of the fitting results is less than 5% except for the case with 0.2 A applied current. The RMSE of the fitting results for the case with 0.2 A applied current is ~6%. Therefore, the accuracy of this model for a constant current input is good and can be used to develop a force-current model.

Table 2 compares the estimated and fitting parameters in the case with 1 Hz sinusoidal excitation and an amplitude of 10 mm. As shown, all parameters are in the same order with fitted values and exhibit the same trend after the fitting. This indicates that using the estimated parameters as initial values can retain the characteristics of these parameters. For the arguments of the hyperbolic tangent function, it is clear that they are almost steady in most cases. This feature will benefit the development of its inverse model.

2.3. Force-Current Model of MR Damper. To derive the force-current model of an MR damper, the first step is to create an MR model for a constant current to be extended into a model for time-varying currents. A simple method to establish the force-current model is by refining the main parameters of the algebraic hyperbolic tangent model as a function of current. It is noteworthy that a practicable inverse model can be derived easily from a force-current model if the parameters in the hysteretic component are a constant value, which avoids solving the inverse of the hyperbolic tangent function. In fact, in parameter identification, the fluctuation of arguments a_1 and a_2 with applied currents for each case is small (shown in Table 2), and the trend for different loading cases depends on the loading amplitude and frequency.

Considering the fluctuating trend of arguments a_1 and a_2 on the applied current i, a piecewise fitting method was employed to refine the other parameters because the relationship between the yield stress of the MR fluid and the applied current changed abruptly around the current of 0.2 A. To further mitigate the effects of arguments a_1 and a_2 on the accuracy of the force-current model, a constrained nonlinear optimization was performed to adjust arguments a_1 and a_2 on the premise that other parameters were provided. The stiffness coefficient k was set as a constant owing to its minor effect on the accuracy of the force-current model. The offset of the damper force f_0 was set as a function of the applied current owing to its steady effect on the accuracy of the force-current model. These parameters were selected as quadratic functions of the applied current. The values determined for these parameters in the case with 1 Hz sinusoidal excitation and an amplitude of 10 mm are listed in Table 3. The RMSE results for various loading cases are shown in Figure 2. The RMSE of the model with constant current in Table 1 is plotted in Figure 2 (refer to constant label). As shown, the RMSE of the piecewise fitting (refer to piecewise label) is slightly larger than that of the model for a constant current. The maximum RMSE is less than 7%.

3. Indispensable Factors in Experimental System

To achieve good accuracy for tracking the control force in real time, a study on the indispensable factors in experimental systems is presented in this section. It is noteworthy that along with the time-varying current input, the dynamic response time must be considered owing to the significant effect of real-time force tracking. This response time is induced by the dynamics of the current driver and the inductance in the electromagnetic coil. According to the study by Jiang and Christenson [30], the inductance of the electromagnetic coil of the MR damper dominates the response time. In this study, only the dynamics of the inductance of the electromagnetic coil is considered. Furthermore, the time lag yielded by the communication and servohydraulic actuator in the experimental systems was considered.

3.1. Experimental Setup. The validated tests for the model-based force tracking scheme were evaluated in an experimental setup designed to produce a displacement in the piston and control the current signal corresponding to the desired force. This setup includes a force tracking scheme in the Simulink module of Matlab, dSPACE® device (dSPACE Corporation), Wonder Box® device (input: 0–5 V, output: 0–2 A, Lord Corporation), and MR damper (Lord Corporation) mounted on a computer-controlled MTS machine (MTS Systems Corporation). The experimental setup is shown in Figure 3.

The RD-8040-1 MR damper utilized in this experiment has a stroke of ±2.5 cm and a resistance of 5 Ω. Its

Table 1: RMSE for estimated and fitting results under different sinusoidal excitations.

Current (A)	1 Hz5 mm		2 Hz5 mm		1 Hz10 mm		2 Hz10 mm	
	Est.	Fit.	Est.	Fit.	Est.	Fit.	Est.	Fit.
0.0	0.145	0.030	0.095	0.033	0.121	0.029	0.118	0.025
0.2	0.142	0.064	0.085	0.064	0.091	0.055	0.095	0.054
0.4	0.100	0.039	0.095	0.041	0.076	0.035	0.090	0.039
0.6	0.091	0.038	0.070	0.039	0.078	0.033	0.084	0.034
0.8	0.092	0.041	0.086	0.045	0.084	0.035	0.087	0.038
1.0	0.103	0.045	0.096	0.046	0.095	0.038	0.084	0.039

Table 2: Model parameters under harmonic excitation.

Current (A)	f_y (N) Est./Fit.	c (N/mm·s) Est./Fit.	k (N/mm) Est./Fit.	f_0 (N) Est./Fit.	a_1 Est./Fit.	a_2 Est./Fit.
0.0	96.4/83.0	0.70/0.71	0.11/0.46	−12.1/−11.7	0.0982/0.1210	0.0314/0.0542
0.2	226.9/198.9	1.21/1.33	0.20/0.27	−16.0/−15.7	0.0663/0.0859	0.0567/0.0751
0.4	500.8/472.7	2.33/2.01	0.18/0.12	−22.9/−23.4	0.0595/0.0799	0.0542/0.0792
0.6	739.2/705.7	3.16/2.55	0.50/0.17	−21.6/−23.0	0.0547/0.0745	0.0552/0.0818
0.8	891.9/847.1	3.82/2.91	0.19/0.27	−20.5/−23.1	0.0523/0.0748	0.0549/0.0811
1.0	1014.1/965.3	4.79/3.72	0.62/0.34	−19.8/−25.9	0.0493/0.0719	0.0539/0.0818

Table 3: Parameter identification results in piecewise fitting way.

Parameters	0–0.2 A	0.2–1 A
f_y (N)	$579.6i + 82.96$	$-719.6i^2 + 1817i - 135.7$
c (N/mm·s)	$3.1i + 0.71$	$0.1429i^2 + 2.669i + 0.84$
f_0 (N)	$-19.95i - 11.77$	$16.28i^2 - 29.55i - 11.67$
k (N/mm)	0.27	0.27
a_1	0.100	0.075
a_2	0.065	0.080

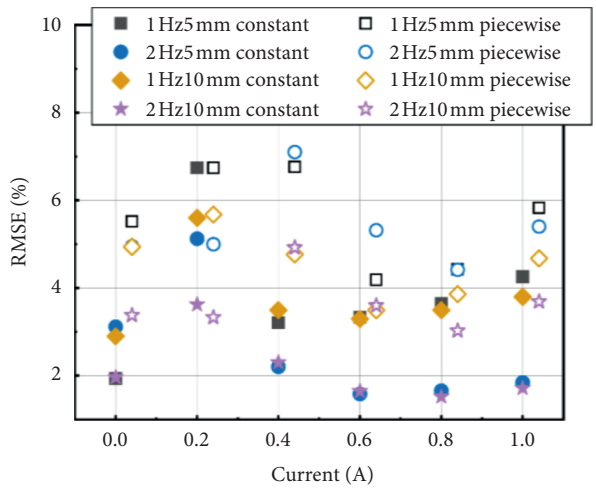

Figure 2: RMSE comparison for various cases.

continuous operating current was limited to 1 A, and its instantaneous current was limited to 2 A. The dSPACE® device was employed for real-time data acquisition (such as measured force f_{act}) from the MTS machine and for motor control by sending control signals (such as displacement signal x) to an external command in the MTS controllable computer. The experimental data were recorded at 1000 Hz sampling frequency. And it should be noted that a low-pass filter is used to process the acquired data by removing the system noise above 20 Hz, which is not used to perform the experiment. The MTS machine was driven by a servohydraulic system that could exert large axial loads onto the test specimen. The Wonder Box® device was used to generate a current i_{act}, which is input to the damper to avoid the current delay in the coil compared to using a voltage-driven power. It is noteworthy that a linear transform occurred in the control voltage and current, as determined by the force tracking scheme, and the transform relationship corresponded to the characteristics of the Wonder Box®.

3.2. Time Delay in Experiments. The experimental system as shown in Figure 3 is a powerful and typical setup to test MR damper characteristics and control MR dampers in real time. In this approach, the displacement signal is applied to the MR damper through an MTS control computer and received by a servohydraulic actuator, while the current signal is only passed through the Wonder Box®. Additionally, the response time induced by the electromagnetic coil and additional response time can be introduced by the communication and servohydraulic actuator to be used for applying signals at each step of the experiment. Herein, a constant time lag by the communication and servohydraulic actuator will be considered.

Figure 4 shows the normalized commands and measured step response from a test where the MR damper is subjected to a step command current, while the piston of the damper moves sinusoidally. The period of the current command is half the period of the displacement command, while the change moment of the step-down (Case A) or step-up current (Case B) coincides with the moment of the maximum displacement command. These conditions occurred because the electromagnetic behavior might be more

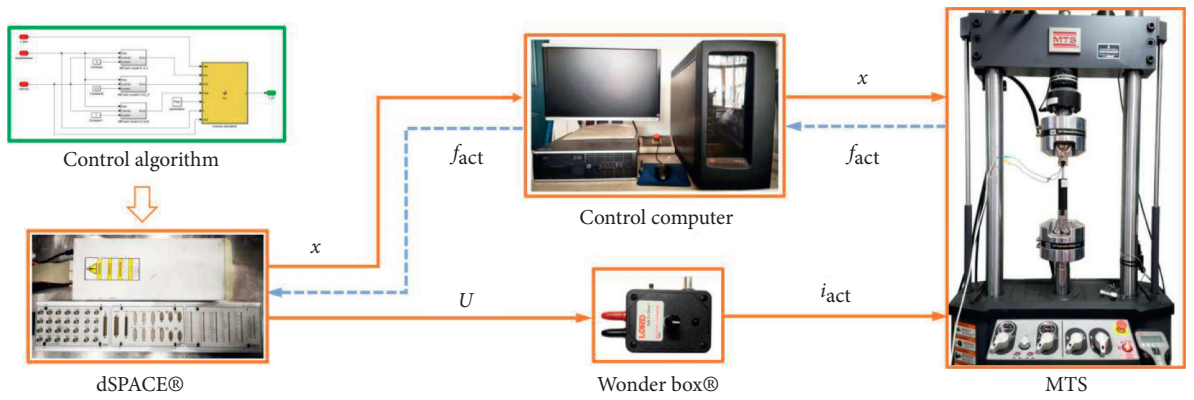

Figure 3: Experimental setup.

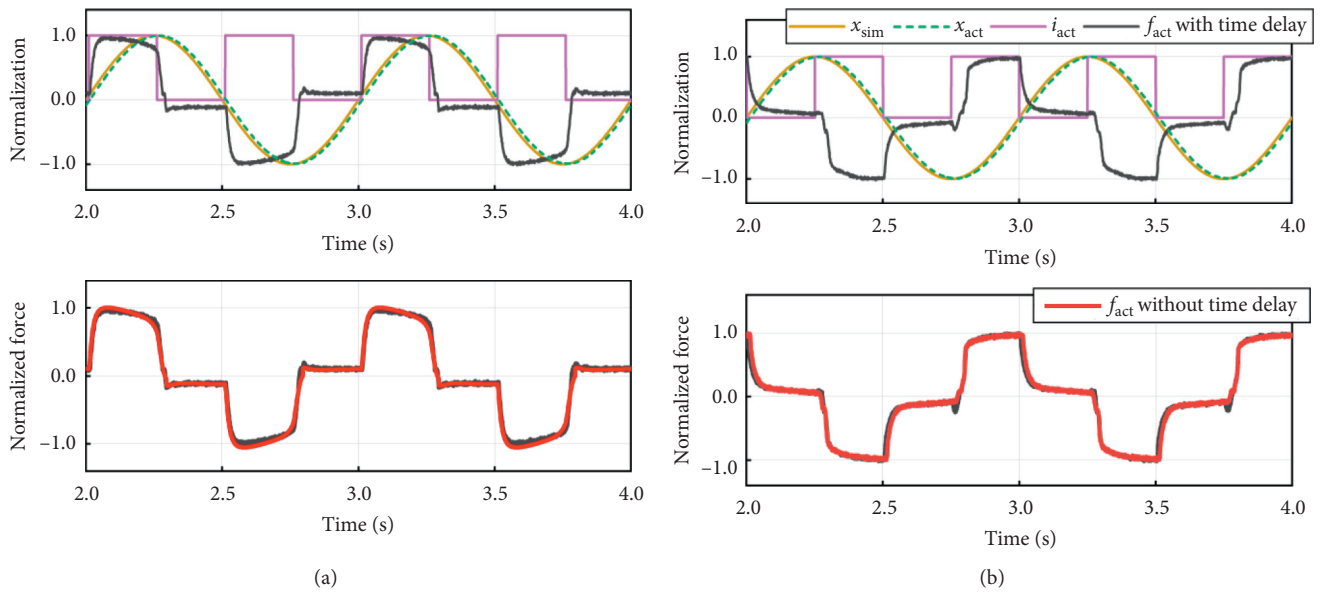

Figure 4: Normalized inputs and responses. (a) Case A. (b) Case B.

prevalent at the moment of piston rebound. Additionally, both step-down and step-up currents exist for these two cases. The command current changes at the middle and end of piston travel.

It should be noted that the command for the MTS machine is the displacement, while the actual travel of MTS is acquired. Thus, the response time of actuator can be represented by the comparison of the command and acquired displacement signal. A time lag between the command displacement signal x_{com} and corresponding measured signal x_{act} is shown in Figure 4, and it can be calculated that the measured time lag is approximately 10 ms. This time lag induces measured force f_{act} peaks at the step-up moment of the current command i_{act}, while the displacement is approximately the maximum negative value. At this moment, the current of the MR damper increases to the maximum current, and the actual motion of the piston has not rebounded owing to the time lag. A current step occurred in the measured force peaks before the piston rebounded. However, this phenomenon did not occur at the maximum positive value. After considering this time lag, the measured force peaks vanished, as shown in Figure 4(b). Although the time lag by the communication and servo-hydraulic actuator was short in this experimental system, it affected the tracking performance near the maximum displacement significantly.

As shown in Figure 4(b), the measured force response could not reach the maximum/minimum force simultaneously owing to the sudden change in the current command. When the current command changed, a countermagnetic field that opposed the original magnetic flux was generated owing to the eddy current in the conductor material. This countermagnetic field delayed the formation of the original magnetic field and hence decelerated the response of the MR damper with time-varying currents. This was because the force-current model of the MR damper above did not consider the inductance in the electromagnetic coil, which was developed based on the response of an MR damper with a constant current.

3.3. Electromagnetic Model. In fact, the accuracy of force tracking depends on the accuracy of the varying-current mechanical model and the electromagnetic dynamic behavior of the MR damper. When the applied current of MR damper varies, the induced eddy current will yield a variable time delay on the real-time current. This problem has been investigated by many researchers [30, 31]. An electromagnetic model including two first-order filters has been used by Chae et al. [32] to model the eddy current effect and the nonlinear hysteretic behavior of damper material magnetization, which can describe the damper force precisely when the force varied suddenly. Furthermore, Chen et al. [33] proposed a dual-loop adaptive control to address the response time delay to consider the electromagnetic dynamic transformation associated with MR devices. Friedman et al. [34] proposed a methodology that applies the overdriving and backdriving of the commands to account for the dynamics of the large-scale MR damper to improve the response time of the device in real time. In this study, a first-order dynamic model was utilized to represent the dynamics of the electromagnetic coil, which can be expressed as

$$\frac{\mathrm{d}i_{\mathrm{sim}}}{\mathrm{d}t} = \nu\left(i_{\mathrm{act}} - i_{\mathrm{sim}}\right), \tag{9}$$

where ν is a constant factor, which can be obtained by minimizing the error between the force of the force-current model and the actual force; i_{act} is the actual command current input to the MR damper; and i_{sim} is the output current of this first-order dynamic model. In fact, i_{sim} is a virtual current to represent the instantaneous magnetic field and can be used directly to predict the damper force by the force-current model. For a given force, the time-varying current can be calculated through its inverse model. If the force-current model is precise, the constant magnetic field generated by this calculated current must be same as the actual instantaneous magnetic field in the MR damper. Therefore, the electromagnetic model can be obtained approximately by fitting a dynamic model to minimize the error between the simulated force of the force-current model and the actual force for any given time-varying current. The factor ν is identified as $50\,\mathrm{s}^{-1}$ in this paper.

Figure 5 shows the time histories of the actual and simulated forces with/without electromagnetic effects. Here, the test conditions are the same as those in Section 3.2. As shown, the error between the simulated and actual forces f_{act} can be reduced by considering electromagnetic effects. For both cases, the simulated force f_{sim} with electromagnetic effects (refer to blue lines) is almost identical with the actual force when the current steps at the middle of piston travel, regardless of whether the current steps up or down. However, it can be seen that the simulated force with electromagnetic effects cannot match the actual force well when the current steps at the end of piston travel as shown in Figure 5(c).

When the current steps down at the end of piston travel, small force peaks appear in the time history of the actual force, while this phenomenon does not occur when the current steps down at the middle of piston travel. This is because the fast movement of the piston can enhance the chain breaking of magnetic particles filled in the annular orifice of the damper at the middle of piston travel. By contrast, the movement of the piston is slower at the end of piston travel, and the weakened chains of magnetic particles yield small force peaks. This phenomenon is known as residual magnetism.

When the current steps up at the end of piston travel, undesired force peaks appear in the simulated force. This is because a discontinuous force response appears at the end of piston travel for discrete constant-current tests. Figure 5(c) shows an enlarged picture of the force-displacement relationship at the end of piston travel. The gray lines are the results of the discrete constant-current tests. The damper forces at the end of piston travel for various constant currents are differed significantly. Therefore, the resulting force-current model based on discrete constant-current tests cannot represent the actual force change with a step-up current at the end of piston travel.

Figure 6 shows the test results when the current command is a random step signal. As shown, the simulated force is almost identical with the actual force in Figure 6(b), and the RMSE between the actual and simulated forces is ~9%. The consequent force-velocity and force-displacement relationships indicate reasonable agreements. Therefore, the first-order dynamic model is suitable for describing electromagnetic effects.

4. Scheme and Performance of Inverse Model-Based Force Tracking

Based on the previous force-current model, constant time lag, and electromagnetic model, an inverse model-based force tracking scheme is proposed to achieve the desired control command in this section. The complete diagram to realize the real-time force tracking is shown in Figure 7. According to the desired control force f_{des}, the inverse force-current model and equivalent inverse electromagnetic model are derived to calculate the desired real-time current. The inverse force-current model can be obtained directly by inverting the force-current model given in Table 3, and the inverse EM model can be calculated through inverting the first-order EM model given in equation (9) with zero initial state. Subsequently, the constant time lag is introduced to consider the response time of the communication and servohydraulic actuator in the experimental system. In Figure 7, i_{sim} is the simulated current calculated directly by the inverse force-current model, and then i_{act} is obtained through an inverse electromagnetic (EM) model, which is the actual current input to the MR damper. In addition, a 10 ms time delay is considered in this scheme by delayed current relative to displacement signal.

4.1. Inverse Model-Based Force Tracking Scheme. To track the control command by the MR damper, two intrinsic constraints must be considered: the passivity and limitation constraints. The passivity constraint means that any force in the active control can be produced regardless of the

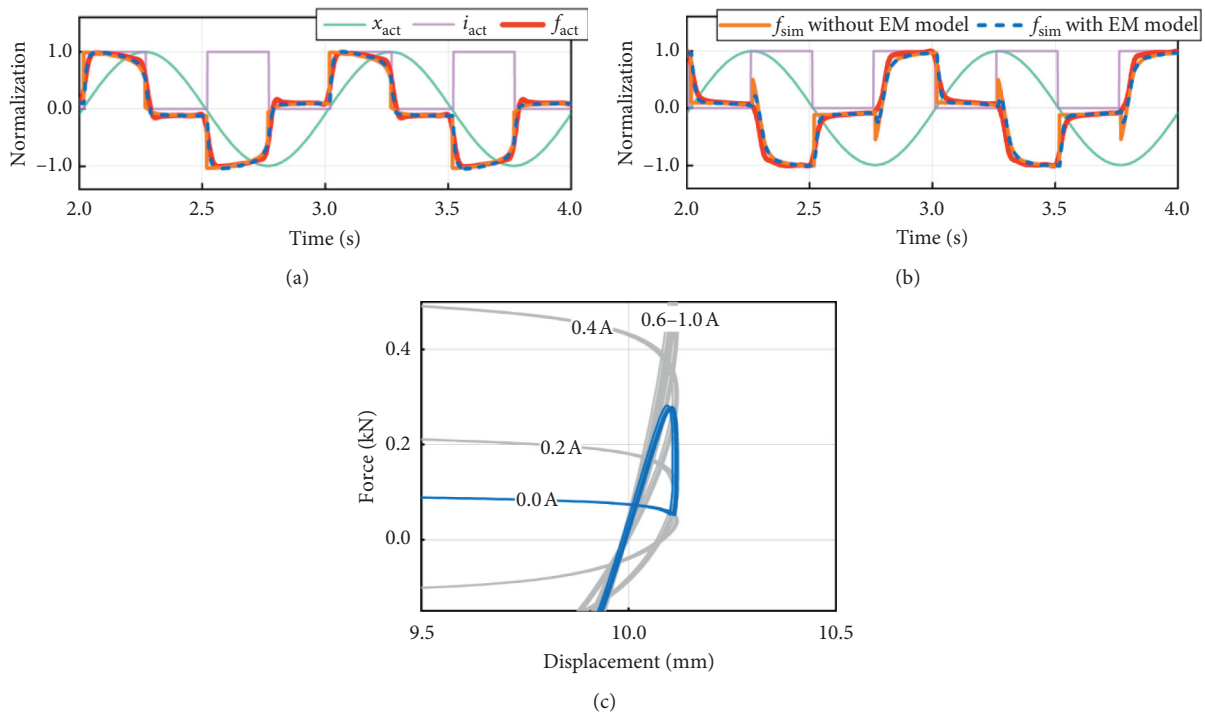

Figure 5: Electromagnetic phenomenon for step current input. (a) Case A. (b) Case B. (c) Force versus displacement for Case B.

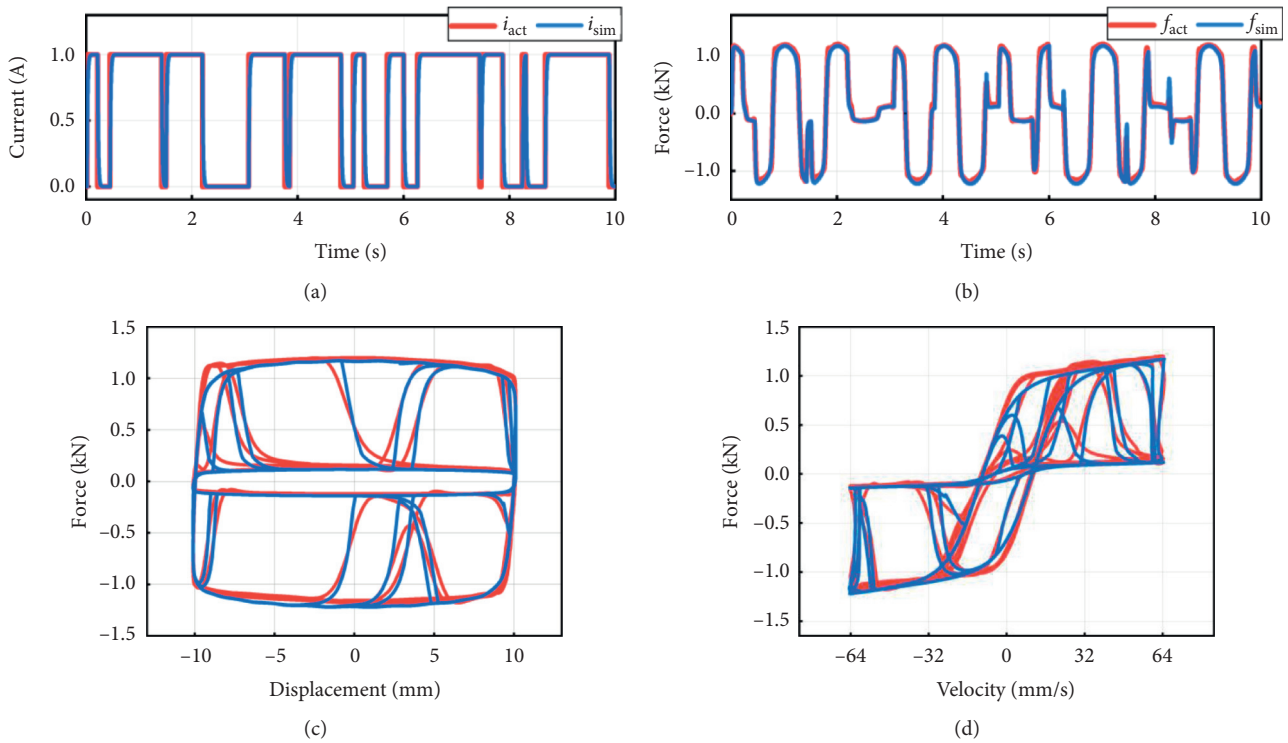

Figure 6: Comparison results for random step current input. (a) Step current. (b) Comparison of historical force. (c) Force versus velocity. (d) Force versus displacement.

relationship between the command force and velocity, while the MR damper can only produce a force to prevent the motion of the structure. For the limitation constraint, the realizable force is limited by the maximum and minimum forces of the MR damper, which is dependent on the instantaneous motion of the piston and the input current.

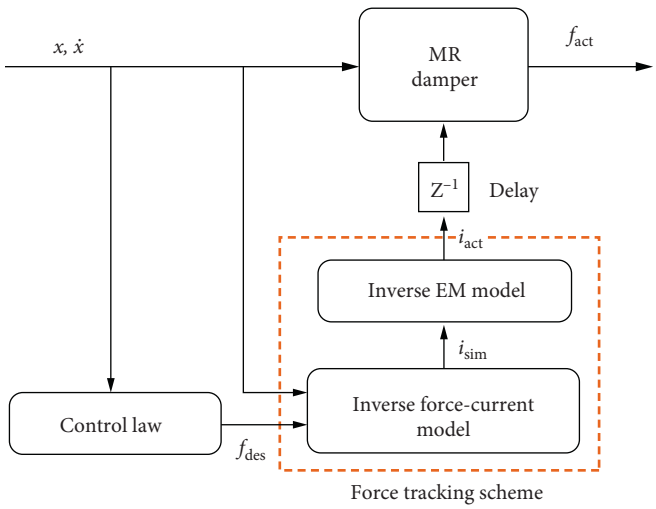

FIGURE 7: Experimental schematics of inverse model-based force tracking scheme.

Consequently, the actual control current for force tracking can be formulated as

$$i_{act} = \begin{cases} 0, & f_{des} f_{sim} < 0 \text{ or } |f_{des}| \le |f_{sim}|^{min}, \\ i_{max}, & |f_{des}| \ge |f_{sim}|^{max} \text{ and } f_{des} f_{sim} > 0, \\ i_{sim}, & \text{others}, \end{cases} \quad (10)$$

where i_{max} is the limited continuous current of the MR damper; i_{sim} is the current derived from the inverse force-current model while the simulated force is in the achievable range of the MR damper; and $|f_{sim}|^{min}$ and $|f_{sim}|^{max}$ are the minimum and maximum simulated forces of the force-current model, respectively.

Assume that control schemes with variable damping and stiffness are a promising approach in semiactive control. MR dampers are typically employed to track the desired damping and stiffness. Therefore, the desired force can be defined as

$$f_{des}(t) = k_{des} x(t) + c_{des} \dot{x}(t), \quad (11)$$

where k_{des} and c_{des} are the desired stiffness coefficient and viscous coefficient, respectively.

4.2. Force Tracking Performance. Based on the control law in equation (11), various pairs of k_{des} and c_{des} are selected to realize a series of experiments for testing the accuracy of the proposed inverse model-based force tracking scheme. All the combinations of k_{des} and c_{des} can be classified into three types: viscous, positive stiffness, and negative stiffness, which encompasses all types of control forces currently. A comparison of the desired force f_{des}, simulated force f_{sim}, and corresponding actual force f_{act} is shown in Figure 8 to visualize the track accuracy. The gray lines of f_{con} are the simulated trajectories for various constant currents.

As shown in Figure 8, the actual force f_{act} matches the achievable force f_{sim} well for most points in the loop. For the viscous and negative stiffness cases, both the relationships of force-velocity and force-displacement show good agreement. For the positive stiffness case, a mismatch appears around the ends of piston travel. To further investigate the mismatch, the tracking process is partitioned into three regions according to the fluctuating directions of the command current, as shown in Figure 9. Region I represents the episode with constant current, where the current is equal to zero or i_{max}, as formulated in equation (10). Region II represents the episode with a continuously varying current, where the current is equal to i_{sim}. Region III represents the episode with a step current, where the current switches between zero and i_{max}. This duration for region III is from the step moment to the moment reaching 95% of the simulated force in the next region.

Figure 9 shows the typical patterns of current for various combinations of k_{des} and c_{des}. For the viscous case, the sequence of the command current is I⟶II in the loop. For the positive and negative stiffness cases, the sequence of the command current is I⟶III⟶I⟶II in the loop. It is noteworthy that the maximum current through the inverse electromagnetic model may exceed the limited continuous current (as shown in Figure 9(c)); subsequently, the current limitation was set to 1.2 times the maximum current i_{max}.

The RMSEs in each loop and different regions are shown in Table 4. As shown, the RMSE of the force tracking scheme is larger than that of the force-current model in Section 2. The largest RMSE of the force tracking scheme is less than 15%.

In region I, the command current is constant, which results in a constant magnetic field. Therefore, the force tracking errors in this region primarily depend on the accuracy of the force-current model for a constant current level (referred to as model errors). The consequent RMSE of the force tracking scheme in this region is less than 7%, which is similar to that of the force-current model.

In region II, the current is directly calculated using the inverse force-current model. The desired control force varies continuously in this region, while the applied current is derived by the combined model of the force-current and electromagnetic models. Figure 10 shows the comparison of i_{sim} by the force-current model and i_{act} by the combined model. As shown, i_{sim} is piecewise continuous in region II, while some steep changes occurred in i_{act} in this region. The consequent RMSE of the force tracking scheme in this region varies from 3% to 11%. For most of the test cases, the RMSE of the force tracking scheme in this region is less than 6%. As shown in Figure 9, such larger force tracking errors are induced because the applied current during the increasing stage of this region is not sufficiently large, which yields a small damper force (referred to as electromagnetic errors). The electromagnetic errors imply that the electromagnetic model based on the step current is not suitable for cases with progressively increasing currents. In addition, the force tracking results during the descending stage of this region are good. In addition, it can be seen that the desired force is exactly equivalent to the simulated force in this region, while the force is outside dissipative domain of the MR damper, so the RMSE in this region can also be regarded as the comparison results between actual force and the desired force.

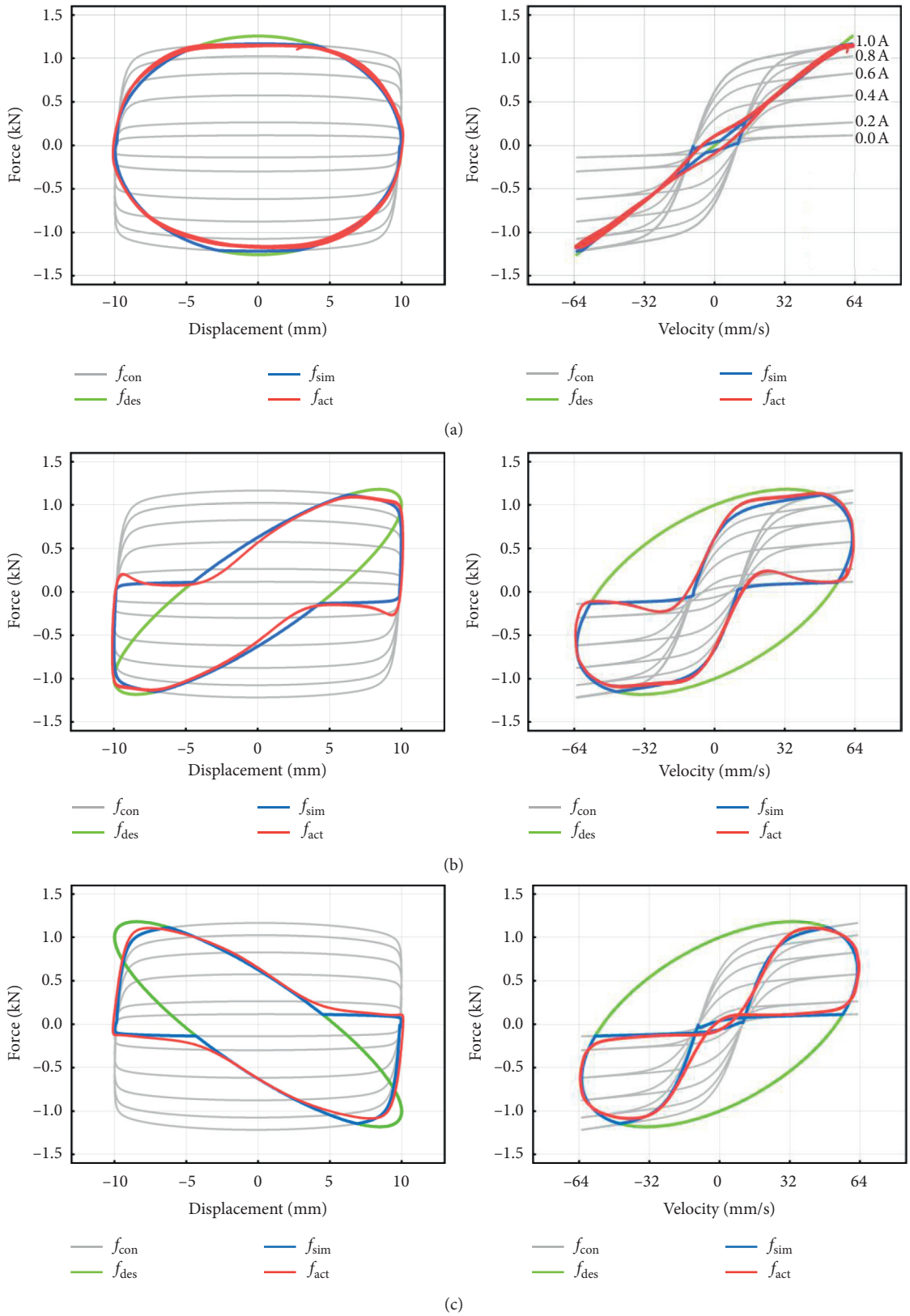

FIGURE 8: Partial results of force tracking scheme. (a) Viscous case (c_{des} = 10 N/m · s). (b) Positive stiffness (c_{des} = 10 N/m · s, k_{des} = 100 N/m). (c) Negative stiffness (c_{des} = 10 N/m · s, k_{des} = −100 N/m).

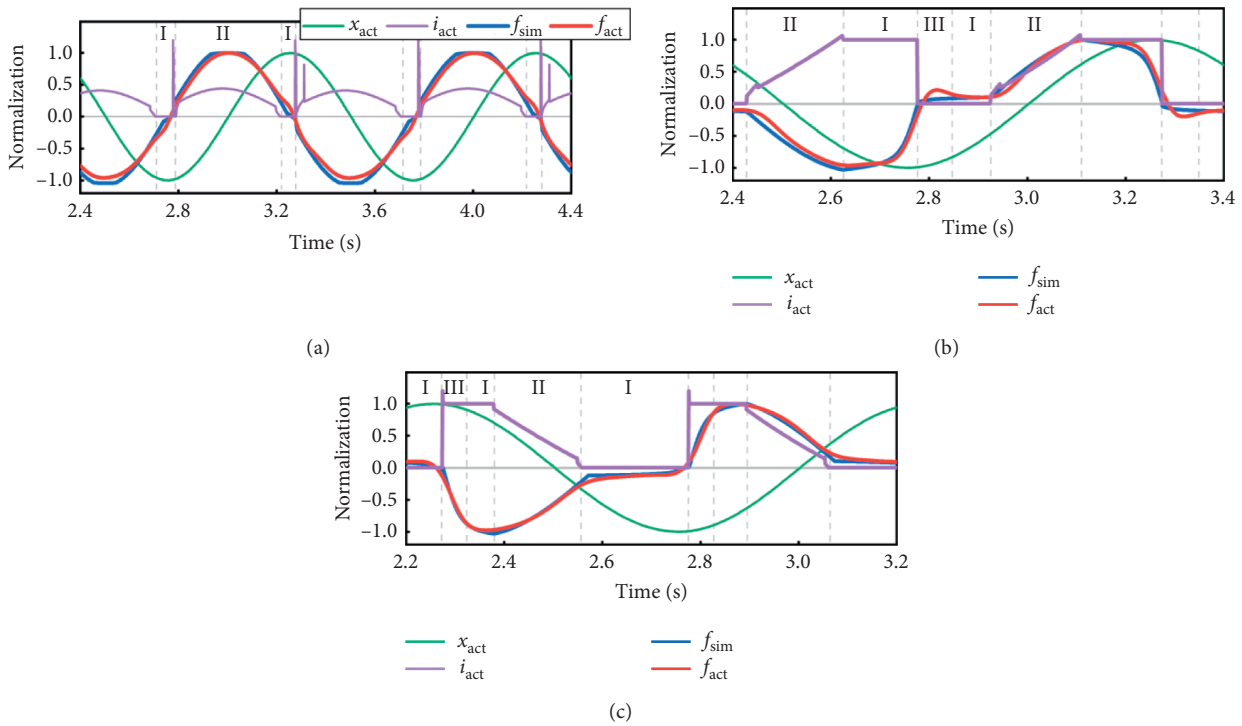

FIGURE 9: Partial results of force tracking scheme. (a) Viscous case (c_{des} = 10 N/m · s). (b) Positive stiffness (c_{des} = 10 N/m · s, k_{des} = 100 N/m). (c) Negative stiffness (c_{des} = 10 N/m · s, k_{des} = −100 N/m).

TABLE 4: RMSE between f_{sim} and f_{act} for different control laws.

Control law		RMSE			
k_{des} (N/m)	c_{des} (N/m · s)	Total	Region I	Region II	Region III
0	10	0.111	0.041 (28.5%)	0.103 (71.5%)	—
0	20	0.057	0.031 (39.2%)	0.048 (60.8%)	—
50	10	0.134	—	0.114 (61.2%)	0.071 (37.8%)
50	20	0.066	0.030 (26.8%)	0.047 (42.0%)	0.035 (31.2%)
100	10	0.114	0.067 (33.8%)	0.066 (33.3%)	0.065 (32.9%)
100	20	0.092	0.062 (39.5%)	0.043 (27.4%)	0.052 (33.1%)
−50	10	0.098	0.029 (19.1%)	0.085 (55.9%)	0.038 (25.0%)
−50	20	0.054	0.028 (30.1%)	0.034 (36.6%)	0.031 (33.3%)
−100	10	0.067	0.022 (20.0%)	0.052 (47.3%)	0.036 (32.7%)
−100	20	0.060	0.028 (27.4%)	0.043 (42.2%)	0.031 (30.4%)

In region III, the current steps to the maximum value for the negative stiffness case or steps to zero for the positive stiffness case. These current steps occurred near the end of piston travel. This means that the electromagnetic effect dominates in this region. Force peaks owing to the residual magnetism and discontinuous force of the force-current mode at the end of piston travel, as discussed in Section 3, may affect the force tracking performance. The resultant RMSE of the force tracking scheme in this region is less than 8%. Owing to the effect of residual magnetism (referred to as RM errors), which occurs when the current steps down at the end of piston travel, the RMSE for the positive stiffness case is much larger than that for the negative stiffness case. However, force peaks owing to the discontinuous force of the force-current mode at the end of piston travel do not occur, as shown in Figure 9(c), which are supposed to appear when the current steps up at the end of piston travel. The time histories of piston displacement and applied current in Figure 9 show that the step moment of the applied current is slightly later than the moment of maximum displacement command. In fact, a time lag exists between the maximum desired force and maximum displacement by the effects of viscous items in the desired force.

In addition to the force tracking errors in these three regions, a clear difference between the actual and simulated forces is observed in the switch between regions I and II. For the positive stiffness case, the current switches from region I to II. For the negative stiffness case, the current switches

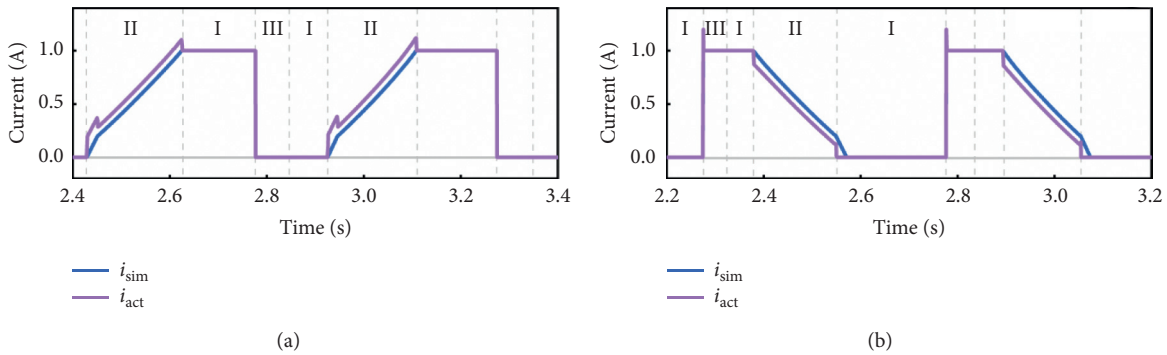

Figure 10: Comparison of i_{sim} and i_{act}. (a) Positive stiffness ($c_{des} = 10\,\text{N/m} \cdot \text{s}, k_{des} = 100\,\text{N/m}$). (b) Negative stiffness ($c_{des} = 10\,\text{N/m} \cdot \text{s}, k_{des} = -100\,\text{N/m}$).

Table 5: Error comparison of different models and schemes.

Model and scheme	Current type	RMSE	$\text{Err}_f^{\text{rms}}$	$\text{Err}^{\text{energy}}$
Proposed in this research	Continuously varying	0.0853	0.0584	0.0399
FF[a] scheme by Weber [24]	Continuously varying	—	—	0.0733*
FB[b] scheme by Weber [24]	Continuously varying	—	—	0.0441*
FFFB[c] scheme by Weber [24]	Continuously varying	—	—	0.0236*
Bouc–Wen model [30]	Step	—	0.1349	0.0409
Fully dynamic model [31]	Step	—	0.0561	0.0283
Variable current MNS[d] model [32]	Step	0.1163	—	—
Lumped parameter model [35]	Constant/continuously varying	—	0.0927	—
Ha model [35]	Constant/continuously varying	—	0.1037	—

[a]Feed forward (FF) force tracking control schemes. [b]Feedback (FB) force tracking control schemes. [c]Combined feed forward/feedback (FFFB) force tracking control schemes. [d]Maxwell nonlinear slider (MNS) model. *The errors are recalculated according to the data in research [24].

from region II to I. For the viscous case, both switches occurred. When the current switches from region I to II, the resulting actual force is less than the desired force, and a larger current should be input. This can be contributed to electromagnetic errors. When the current switches from region II to I, the resulting actual force is larger than the desired force. This can be attributed to RM errors.

To summarize, model, electromagnetic, and RM errors occurred for the viscous and positive stiffness cases, while model and RM errors occurred for the negative stiffness case. Electromagnetic and RM errors dominate the force tracking performance and constitute ~70% of the total error. To mitigate electromagnetic errors, a different electromagnetic model from that one obtained by the step current should be developed to consider the progressively increasing current. To mitigate RM errors, a back-driven current should be developed to break the chains of magnetic particles rapidly by applying an inverse current.

4.3. Error Comparison with Previous Studies. To present the force tracking performance of the MR damper, a comparison with previous studies is necessary. Because only a few published papers have presented the force tracking error, model errors for the time-varying current [30, 32, 35] are introduced to compare with the proposed force tracking scheme. Therefore, the same error evaluation criteria used in previous studies were utilized and expressed as follows:

$$\text{Err}_f^{\text{rms}} = \frac{\sqrt{(1/N)\sum_{j=1}^{N}\left(f_{\text{act}}^{j} - f_{\text{sim}}^{j}\right)^2}}{f_{\text{act}}^{\max}}, \tag{12}$$

$$\text{Err}^{\text{energy}} = \frac{\left|E^{\text{act}} - E^{\text{sim}}\right|}{E^{\text{act}}}, \tag{13}$$

where $f_{\text{act}}^{\max}$ is the maximum damper force from experimental data; E^{act} and E^{sim} are the energies absorbed by the damper in the experiment and simulation during an event, respectively, which are calculated by summing up the areas under the damper force-displacement curve; $\text{Err}_f^{\text{rms}}$ represents the normalized force tracking error to the actual peak force; and $\text{Err}^{\text{energy}}$ represents the normalized absorbed energy error to the actual absorbed energy. The results compared with previous studies are shown in Table 5.

It is noteworthy that $\text{Err}^{\text{energy}}$ for the method by Weber is not the direct results presented in his study. $\text{Err}^{\text{energy}}$ was recalculated according to the data in [24]. The RMSE of the proposed method in this study is the mean value for all pairs of k_{des} and c_{des} listed in Table 4. As shown in Table 5, the proposed force tracking scheme provides a small RMSE. $\text{Err}_f^{\text{rms}}$ is less than 6% and $\text{Err}^{\text{energy}}$ is less than 4%. The RMSE results of the proposed method show reasonable accuracy. For different control forces, the proposed method in this study can achieve a good performance over the range of limiting forces generated by the MR damper. Moreover, the

main advantage of the proposed force tracking scheme is its ability to explicitly derive the current in real time according to the desired force.

5. Conclusions

An inverse model-based force tracking scheme that could track the desired force with different viscosities and stiffnesses was presented. The algebraic hyperbolic tangent model was utilized to establish a force-current model, and a methodology was developed to evaluate the characteristic parameters that defined the model for a constant current input, which considered the individual effect of each term of the model. Meanwhile, the time delay in the actuator was measured, and the dynamic electromagnetic behavior in the MR damper for a time-varying current input was considered by a first-order electromagnetic model.

Numerous validation experiments were performed to track the force with different viscosities and stiffnesses. The results indicated that the performance of the inverse model-based scheme was good. This scheme can be regarded as an effective and reliable approach for tracking the desired force in real time. Its main advantage is its ability in explicitly deriving the real-time command current.

Further analysis on force tracking errors indicated that the accuracy of the scheme primarily depended on the accuracy of the electromagnetic model and residual magnetism effect, which constituted 70% of the total error. The electromagnetic model obtained by the step current was not suitable for the case with progressively increasing currents. The residual magnetism effect was prevalent when the current stepped down at the end of piston travel.

Data Availability

The data used to support the findings of this study are available from the corresponding author upon request.

Conflicts of Interest

The authors declare that there are no conflicts of interest.

Acknowledgments

This study was supported by the National Natural Science Foundation of China (no. 51678210).

References

[1] S. J. Dyke and B. F. Spencer, "A comparison of semi-active control strategies for the MR damper," in *Proceedings of the Intelligent Information Systems IIS*, December 1997.

[2] H. N. Li, Z. Chang, and J. Li, "Semi-active control for eccentric structures with MR damper by hybrid intelligent algorithm," in *Proceedings of the International Conference on Intelligent Computing, ICIC*, Hefei, China, August 2005.

[3] G. Z. Yao, F. F. Yap, G. Chen, W. H. Li, and S. H. Yeo, "MR damper and its application for semi-active control of vehicle suspension system," *Mechatronics*, vol. 12, no. 7, pp. 963–973, 2002.

[4] S. J. Dyke, B. F. Spencer, M. K. Sain, and J. D. Carlson, "Modeling and control of magnetorheological dampers for seismic response reduction," *Smart Materials and Structures*, vol. 5, no. 5, pp. 565–575, 2015.

[5] H. P. Gavin, "Multi-duct ER dampers," *Journal of Intelligent Material Systems and Structures*, vol. 12, no. 5, pp. 353–366, 2001.

[6] B. J. Brent and R. E. Christenson, "System identification of a 200 kN magneto-rheological fluid damper for structural control in large-scale smart structures," in *Proceedings of the American Control Conference*, New York, NY, USA, July 2007.

[7] B. F. Spencer, S. J. Dyke, M. K. Sain, and J. D. Carlson, "Phenomenological model for magnetorheological dampers," *Journal of Engineering Mechanics*, vol. 123, no. 3, pp. 230–238, 1997.

[8] A. Dominguez, R. Stiharu, and I. Sedaghati, "Modelling the hysteresis phenomenon of magnetorheological dampers," *Smart Materials and Structures*, vol. 13, no. 6, pp. 1351–1361, 2004.

[9] A. Dominguez, R. Sedaghati, and I. Stiharu, "A new dynamic hysteresis model for magnetorheological dampers," *Smart Materials and Structures*, vol. 15, no. 5, pp. 1179–1189, 2006.

[10] P. Guo, J. Xie, and X. Guan, "Dynamic model of MR damper based on a hysteretic magnetic circuit," *Shock and Vibration*, vol. 2018, Article ID 2784950, 13 pages, 2018.

[11] H. H. Tsang, R. K. L. Su, and A. M. Chandler, "Simplified inverse dynamics models for MR fluid dampers," *Engineering Structures*, vol. 28, no. 3, pp. 327–341, 2006.

[12] E. R. Wang, X. Q. Ma, S. Rakheja, and C. Y. Su, "Force tracking control of vehicle vibration with MR-dampers," in *Proceedings of the IEEE International Symposium on Mediterrean Conference on Intelligent Control*, Limassol, Cyprus, June 2005.

[13] T. W. S. Chow and Y. Fang, "A recurrent neural-network-based real-time learning control strategy applying to nonlinear systems with unknown dynamics," *IEEE Transactions on Industrial Electronics*, vol. 45, no. 1, pp. 151–161, 2002.

[14] D. H. Wang and W. H. Liao, "Modeling and control of magnetorheological fluid dampers using neural networks," *Smart Materials and Structures*, vol. 14, no. 1, pp. 111–126, 2005.

[15] M. Khalid, R. Yusof, M. Joshani, H. Selamat, and M. Joshani, "Nonlinear identification of a magneto-rheological damper based on dynamic neural networks," *Computer-Aided Civil Infrastructure Engineering*, vol. 29, no. 3, pp. 221–233, 2014.

[16] G. Yan and L. L. Zhou, "Integrated fuzzy logic and genetic algorithms for multi-objective control of structures using MR dampers," *Journal of Sound and Vibration*, vol. 296, no. 1-2, pp. 368–382, 2014.

[17] X. Do, K. Shah, and S. Choi, "Damping force tracking control of mr damper system using a new direct adaptive fuzzy controller," *Shock and Vibration*, vol. 2015, Article ID 947937, 16 pages, 2015.

[18] L.-H. Zong, X.-L. Gong, C.-Y. Guo, and S.-H. Xuan, "Inverse neuro-fuzzy MR damper model and its application in vibration control of vehicle suspension system," *Vehicle System Dynamics*, vol. 50, no. 7, pp. 1025–1041, 2012.

[19] C.-C. Chang and L. Zhou, "Neural network emulation of inverse dynamics for a magnetorheological damper," *Journal of Structural Engineering*, vol. 128, no. 2, pp. 231–239, 2002.

[20] P.-Q. Xia, "An inverse model of MR damper using optimal neural network and system identification," *Journal of Sound and Vibration*, vol. 266, no. 5, pp. 1009–1023, 2003.

[21] Y. Q. Ni, Z. H. Chen, and S. W. Or, "Experimental identification of a self-sensing magnetorheological damper using soft computing," *Journal of Engineering Mechanics*, vol. 247, no. 7, p. 04015001, 2015.

[22] K. A. Bani-Hani and M. A. Sheban, "Semi-active neuro-control for base-isolation system using magnetorheological (MR) dampers," *Earthquake Engineering and Structural Dynamics*, vol. 35, no. 9, pp. 1119–1144, 2006.

[23] F. Weber, S. Bhowmik, and J. Høgsberg, "Extended neural network-based scheme for real-time force tracking with magnetorheological dampers," *Structural Control and Health Monitoring*, vol. 21, no. 2, pp. 225–247, 2014.

[24] F. Weber, "Robust force tracking control scheme for MR dampers," *Structural Control and Health Monitoring*, vol. 22, no. 12, pp. 1373–1395, 2015.

[25] H. Metered, P. Bonello, and S. O. Oyadiji, "The experimental identification of magnetorheological dampers and evaluation of their controllers," *Mechanical Systems and Signal Processing*, vol. 24, no. 4, pp. 976–994, 2010.

[26] G. Yang, *Large-scale magnetorheological fluid damper for vibration mitigation: modeling testing and control*, Ph.D. dissertation, University of Notre Dame, Notre Dame, IN, USA, 2001.

[27] F. Weber, "Bouc-Wen model-based real-time force tracking scheme for MR dampers," *Smart Materials and Structures*, vol. 22, no. 4, p. 045012, 2013.

[28] Q. P. Ha, M. T. Nguyen, J. Li, and N. M. Kwok, "Smart structures with current-driven MR dampers: modeling and second-order sliding mode control," *IEEE/ASME Transactions on Mechatronics*, vol. 18, no. 6, pp. 1702–1712, 2013.

[29] F. Weber, "Semi-active vibration absorber based on real-time controlled MR damper," *Mechanical Systems and Signal Processing*, vol. 46, no. 2, pp. 272–288, 2014.

[30] Z. Jiang and R. E. Christenson, "A comparison of 200 kN magneto-rheological damper models for use in real-time hybrid simulation pretesting," *Smart Materials and Structures*, vol. 20, no. 6, p. 065011, 2011.

[31] Z. Jiang and R. E. Christenson, "A fully dynamic magneto-rheological fluid damper model," *Smart Materials and Structures*, vol. 21, no. 6, p. 065002, 2012.

[32] Y. Chae, J. M. Ricles, and R. Sause, "Modeling of a large-scale magneto-rheological damper for seismic hazard mitigation. Part II: semi-active mode," *Earthquake Engineering & Structural Dynamics*, vol. 42, no. 5, pp. 687–703, 2013.

[33] X. Chen, Y. Li, J. C. Li, and X. Gu, "A dual-loop adaptive control for minimizing time response delay in real-time structural vibration control with magnetorheological (MR) devices," *Smart Materials and Structures*, vol. 27, no. 1, p. 015005, 2018.

[34] A. J. Friedman, S. J. Dyke, and B. M. Phillips, "Over-driven control for large-scale MR dampers," *Smart Materials and Structures*, vol. 22, no. 4, p. 045001, 2013.

[35] D. Case, B. Taheri, and E. Richer, "A lumped-parameter model for adaptive dynamic MR damper control," *IEEE/ASME Transactions on Mechatronics*, vol. 20, no. 4, pp. 1689–1696, 2015.